Ultrafast optical Kerr effect measurements of third-order nonlinearities in cross-conjugated *iso*-polydiacetylene oligomers

Aaron D. Slepkov and Frank A. Hegmann
Department of Physics, University of Alberta, Edmonton, Alberta T6G 2J1, Canada

Yuming Zhao and Rik R. Tykwinski
Department of Chemistry, University of Alberta, Edmonton, Alberta T6G 2G2, Canada

Kenji Kamada
Photonics Research Institute, National Institute of Advanced Industrial Science and Technology (AIST), Ikeda, Osaka 563-8577, Japan

(Received 7 November 2001; accepted 11 December 2001)

We present a study on the ultrafast third-order nonlinearities of a novel series of *iso*-polydiacetylene oligomers (*iso*-PDAs). Unlike polydiacetylenes that contain a linearly-conjugated backbone, *iso*-PDAs have a backbone that is cross-conjugated. A new Kerr-gate technique, differential optical Kerr effect (DOKE) detection, is used to measure third-order nonlinear susceptibilities, $\chi^{(3)}$, and second hyperpolarizabilities, γ, of monomer, dimer, trimer, pentamer, and heptamer samples in tetrahydrofuran (THF) solutions. A linear increase in γ as a function of the number of repeat units is observed for all samples except the monomer, suggesting that the fixed-length linearly conjugated segments dominate the electronic polarizability. An added increase to the oligomer nonlinearities due to communication along the cross-conjugated path is not observed. The largest nonlinearity was observed in the heptamer sample, displaying a second hyperpolarizability relative to the THF solvent of $\gamma_{\text{heptamer}}/\gamma_{\text{THF}} = 181 \pm 9$. In addition, an interesting feature arising out of the signal decay tail is present in the samples but absent in our THF solvent reference. © *2002 American Institute of Physics.* [DOI: 10.1063/1.1447908]

I. INTRODUCTION

For the past 25 years, scientists have searched for materials with high nonlinear susceptibilities and ultrafast response times. One of the main goals of such research is the development of viable all-optical switching devices.[1,2] For practical applications, nonlinear materials will also require sufficient transparency, stability, speed, and processability.[3] Early on, the benefit of delocalized electronic structure has pointed towards π-conjugated organic chromophores and polymers as potential candidate materials. Studies of long, linearly conjugated polyacetylenes[4] and polydiacetylenes[5] have revealed these materials to have very high nonlinearities. Furthermore, studies of the relationship between the third-order susceptibility, $\chi^{(3)}$, and conjugation length have shown that extending the π-conjugated path by increasing the number of double and triple bonds significantly increases the nonlinearities.[2,6,7] However, as the conjugation length increases, the maximum absorption wavelength, $\lambda_{\max}$, increases as well, rendering these materials insufficiently transparent for many practical applications. It is becoming apparent that the current trend of attempting to maximize $\chi^{(3)}$ and second hyperpolarizability, γ, by simply increasing the length of the linearly conjugated backbones of various oligomers will not yield materials of sufficient merit.

Several research groups have identified the need to study a variety of structure-property relationships of π-conjugated materials in an attempt to understand how to better engineer useful materials with high third-order nonlinearities. These groups have studied properties ranging from symmetry and planarity to pendant functionality.[8–12] Modes of conjugation have also been explored, including spiro- and cross-conjugation.[10,13,14] Because π-delocalization is less efficient across a cross-conjugated bridge, studying various aspects of electronic communication in cross-conjugated systems is necessary if we are to understand the important aspects of the nonlinear responses in organic materials. Furthermore, it is important to compare how cross-conjugation contributions to γ correlate with preliminary UV-vis spectroscopic studies that suggest only limited communication.[15] For these reasons we have undertaken to study the effect of cross-conjugation on the third-order nonlinearities of *iso*-polydiacetylene-based oligomers.

II. THE OPTICAL KERR EFFECT

The optical Kerr effect (OKE) is an optically induced birefringence in an isotropic medium.[16] In a standard homodyne Kerr gate,[17–22] an intense, linearly polarized pump pulse, polarized, for example, at 45° to the horizontal, excites a birefringence in an isotropic medium. The change in the index of refraction induced by the pump pulse, $\delta n = \delta n_{\parallel} - \delta n_{\perp}$, between the parallel and perpendicular axes to the pump polarization can be probed by a weaker probe pulse that is polarized, say, horizontally. The induced birefringence, δn, manifests itself as retardation in the probe beam polarization and may be detected by use of a post-sample analyzer. Furthermore, the probe beam may be time delayed with respect to the pump pulse, yielding a temporal profile of the induced birefringence. When the pump pulse

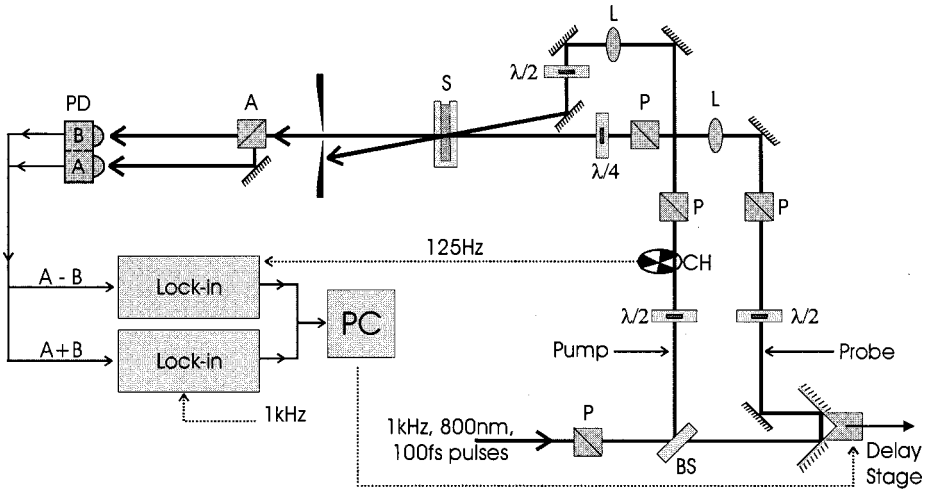

FIG. 1. Schematic of the differential optical Kerr effect (DOKE) detection layout. PD-A: rejected probe beam photodiode detector; PD-B: transmitted probe beam photodiode detector; BS: pellicle beam splitter; λ/4: quarter-wave plate; λ/2: half-wave plate; P: Glan-laser polarizer; A: Glan-laser polarizer acting as an analyzer; L: lens (f=30 cm); CH: chopper operating at 125 Hz; PC: computer; S: 1-mm path length quartz cuvette sample holder.

arrives well before the probe pulse, there is no induced birefringence and no probe light passes through the crossed polarizers. When the two pulses arrive simultaneously at a sample dominated by an ultrafast electronic nonlinearity, the probe beam experiences the maximum rotation in polarization given by

$$\phi = \frac{2\pi d}{\lambda} n_2 I_{\text{pump}}, \tag{1}$$

where n_2 is the nonlinear index of refraction and is proportional to $\chi^{(3)}$, λ is the wavelength, d is the sample length, and I_{pump} is the pump intensity in units of W/m^2. The quantity n_2 can be considered as a modification to the linear index of refraction such that the total index of refraction is given by $n = n_0 + n_2 I_{\text{pump}}$, n_0 being the linear index of refraction. $\chi^{(3)}$ is obtained from n_2 by[23]

$$n_2\left(\frac{m^2}{W}\right) = \frac{3.9\times 10^{-6}}{n_0^2}\chi^{(3)}(\text{esu}), \tag{2}$$

where n_2 is in units of m^{2}W^{-1} and $\chi^{(3)}$ is in esu, the respective units currently in favor.[23] The molecular second hyperpolarizability, γ, may be obtained by[3]

$$\gamma = \frac{\chi^{(3)}}{N_c L^4}, \tag{3}$$

where N_c is the molecular number density in cm^{-3} and L^4 is the Lorentz field-factor which may be approximated by $[(n_0^2+2)/3]^4$ for isotropic liquid media.[24]

Since the homodyne detection scheme operates with crossed polarizers, the detected signal is proportional to the square of the pump intensity. As a consequence, this technique is unable to separate the real and imaginary components of $\chi^{(3)}$. Furthermore, because this detection scheme operates with fully crossed polarizers, the obtained signal is extremely small and may be of the same order or smaller than typical noise levels. In an attempt to separate the real and imaginary components of $\chi^{(3)}$ and to obtain signals much larger than the ambient scatter noise, another detection scheme, optical heterodyne detection (OHD-OKE), is used by many research groups.[25–37] In OHD-OKE, a quarter-wave plate ($\lambda/4$) is placed between the probe polarizer and sample such that the fast axis of the quarter-wave plate is parallel to the polarizer. By slightly rotating the polarizer fast axis, $\pi/2$ out-of-phase light may be added to the probe beam. Depending on the angle chosen for the polarizer, this technique can provide the real or imaginary components of the nonlinear response directly from the Kerr signal. This scheme works in the regime where the transmitted signal is linear with pump intensity.

III. EXPERIMENT

A. Differential optical Kerr effect (DOKE) setup

We have developed a modification to the OHD-OKE scheme. Figure 1 presents a schematic of our differential optical Kerr effect (DOKE) detection setup. The complete description and analysis of this setup will be discussed elsewhere. Briefly, our DOKE setup is similar to various optical biasing schemes routinely used in the field of free-space electro-optic sampling of terahertz pulses.[38,39] The pump and probe pulses are generated by an amplified Ti:sapphire laser producing 800 nm, 100 fs pulses at a 1 kHz repetition rate. A computer-controlled stage is used to vary the delay between the pump and probe pulses. The pump pulse is polarized 45° to the horizontal before being focused onto a 1 mm sample path-length quartz cuvette filled with a sample solution. The much weaker probe beam is initially polarized vertically by a Glan-laser polarizer and then passes through a quarter-wave plate oriented to produce circular polarized light. Typical pump and probe powers at the sample location are between 0.5 and 6 mW for the pump beam and 50–80 μW for the probe beam. The probe light is focused to overlap in the sample with the pump beam at a near coincident angle, $\theta < 5°$. Typical spot sizes for the pump and probe beams are 500 and 240 μm, respectively. The pump beam is blocked post sample while the probe light is allowed to travel to a second Glan-laser polarizer acting as the analyzer. Here, the transmitted and rejected beams are separated and directed to a pair of balanced photodiodes. Photodiode "A" receives the rejected beam, and photodiode "B" receives the transmitted beam. The pump beam is chopped at 125 Hz, and lock-in detection is used to monitor the A−B signal. The A+B

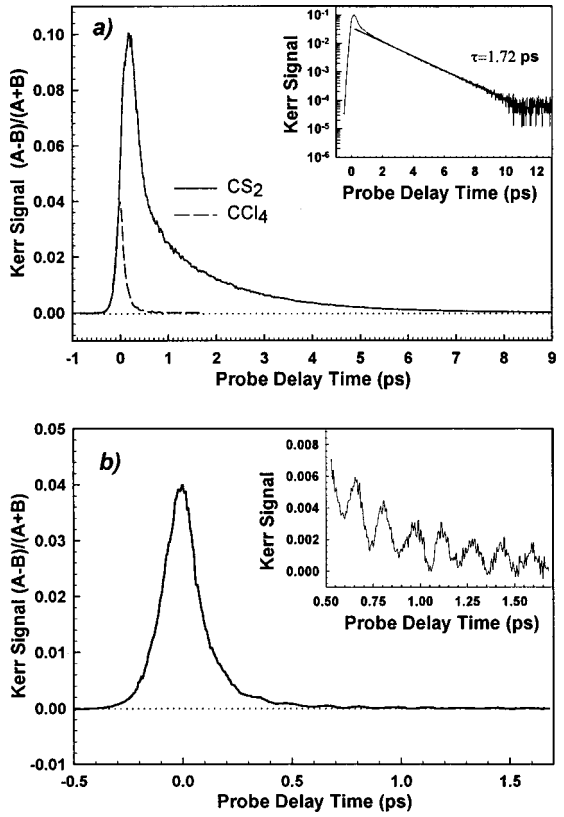

FIG. 2. Kerr signals from CS_2 and CCl_4 standards. (a) CS_2 Kerr response. Inset: semi-log plot showing a 1.72 ps relaxation time (straight line) in the tail of the CS_2 signal. (b) CCl_4 Kerr response. Inset: close-up of the post-peak tail in the CCl_4 response showing the excitation of vibrational modes. The dashed line in (a) is the CCl_4 signal from (b) superimposed for direct comparison to the CS_2 Kerr response.

signal is detected at 1 kHz using a separate lock-in amplifier. Finally, these signals are sent to a computer used for data acquisition and delay-stage control.

The key feature of the DOKE setup is that the A−B detection acts as our Kerr effect signal. If $\mathrm{Im}(\chi^{(3)})$ is small, A+B acts as a probe beam reference. In the presence of nonlinear absorption such as two-photon absorption, the A+B signal provides independent detection of the $\mathrm{Im}(\chi^{(3)})$ processes. The photodiodes are calibrated in such a way that in the absence of any birefringence, A and B signals are equal and A−B is zero.

Consider a vertically polarized probe beam and a sample with an induced birefringence of $\phi=\phi'+i\phi''$, where ϕ' and ϕ'' are the real and imaginary components of the phase retardation, respectively. If after passing through a quarter-wave plate set with fast axis at 45°, the beam is incident on the sample, the detected signal ratio is given by

$$\frac{A-B}{A+B}=\frac{\sin\phi'}{\cosh\phi''}. \tag{4}$$

This relationship is valid when the pump and probe beams are initially polarized at 45° to each other. However, when the pump is polarized vertically (same as the initial probe pulse polarization) the detected signal ratio is

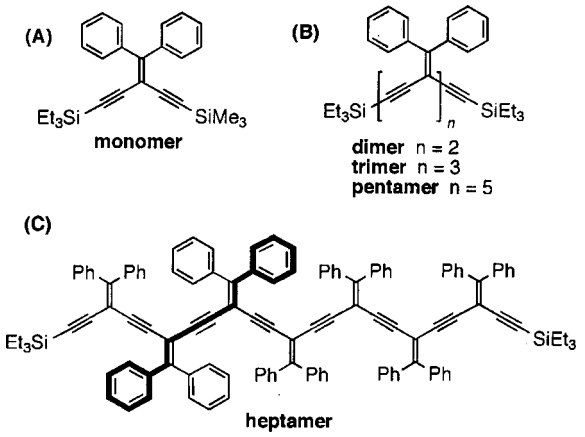

FIG. 3. Chemical structure of the *iso*-polydiacetylene oligomers showing (a) the monomer, (b) the repeat unit, and (c) the heptamer sample. The longest linear conjugated segment present in the $n\geqslant 2$ molecules is shown as a thick line in the heptamer structure.

$$\frac{A-B}{A+B}=\tanh\phi'', \tag{5}$$

and contains only the imaginary contribution to $\chi^{(3)}$. Thus, by alternating between the two pump polarization conditions, it is possible to separate ϕ' and ϕ'' terms, yielding the real and imaginary components of $\chi^{(3)}$. Clearly, in the absence of absorptive nonlinearities, $\phi''=0$, Eq. (5) gives a null signal and Eq. (4) is simply

$$\frac{A-B}{A+B}=\sin\phi', \tag{6}$$

a purely real response.

Much like the heterodyne scheme, DOKE detection obtains signals that are linear with pump and probe intensity. However, the DOKE technique affords a larger dynamic range of linear signal than the typical heterodyne scheme. Furthermore, we have found that in comparison to OHD-OKE, the DOKE signals are larger, making detection easier.

There are numerous factors that hinder the comparison of exact γ and $\chi^{(3)}$ values.[10,11,23,40] To avert many of the pitfalls in reporting exact nonlinearity values, it is extremely useful to report them relative to some reference material. Quite often, that reference material is the solvent. Thus, when reporting exact values obtained from relative values, the values for the reference material should also be reported. Furthermore, simply generating $\chi^{(3)}$ values that are comparable to those reported in the literature may not be a sufficient indication of proper Kerr effect detection. However, there are several typical material responses that can act as verification of proper detection. Two such features are the slow decay tail of the CS_2 Kerr effect signal, shown in Fig. 2(a), and the excitation of vibrational modes in CCl_4, as shown in Fig. 2(b). The long tail in CS_2 shows an exponential decay time of 1.72 ps that is consistent with the CS_2 decay times in the range of 1.7 ps to 1.79 ps reported extensively in the literature.[26,27,35,37,41] In addition, with short optical pulses, the two optically active modes in CCl_4 at 218 and 314 cm^{-1} (Refs. 26, 30, 31, 33, and 41) can be observed as seen in the inset of Fig. 2(b). Figure 2 displays both of

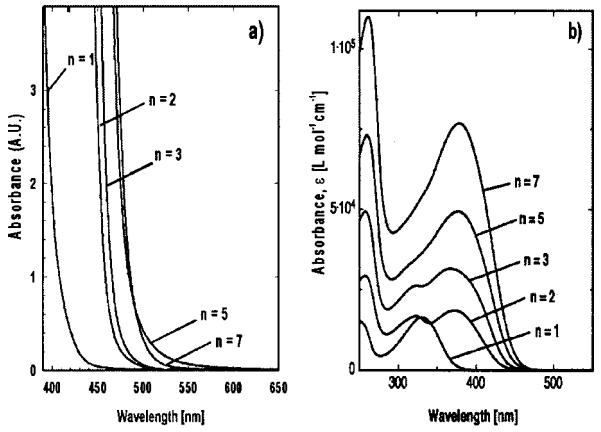

FIG. 4. (a) UV-Vis absorption spectra of the oligomer samples at the concentrations used for the OKE studies. The scale shows that the absorption edge, λ_{max}, has nearly saturated by the heptamer ($n=7$) sample. (b) The full absorption spectrum for the oligomer samples. n is the number of repeat units in the sample.

these features and acts as an indication that our DOKE detection setup compares favorably with others.

B. Sample preparation

For this work, we have synthesized a novel class of *iso*-polydiacetylene (*iso*-PDA) oligomers, as described in Fig. 3. The phenylated *iso*-PDA oligomers were synthesized stepwise using a procedure analogous to that published for alkyl substituted derivatives.[42] All oligomers have been fully characterized by ^{13}C and ^{1}H NMR, IR and UV-Vis spectroscopies, and HRMS. These compounds are stable under ambient conditions and require no special handling precautions. Full synthetic details will be published elsewhere. Samples were prepared by dissolving solid oligomer samples in high-purity tetrahydrofuran (THF) to give solutions of 0.1—0.23 M. Typically, solutions were made to 0.6 mL as the quartz cuvette has a sample path length of 1.0 mm and is able to hold 0.4 mL of solution. Samples were measured for nonlinearities and UV-Vis absorbances within 24 h of sample preparation. The sample nonlinearities were probed at 800 nm, which is far from resonance, as may be seen in Fig. 4.

IV. RESULTS AND ANALYSIS

Table I lists relevant properties and results for the sample series. The DOKE signals for the oligomer series and the

TABLE I. Summary of results for the *iso*-polydiacetylene oligomer series. γ_S and γ_{THF} are the second hyperpolarizabilities of the oligomer samples and THF reference, respectively. n is the number of repeat units in the oligomer

	n	Concentration (M)	$\gamma_S \times 10^{-36}$ esu	$\frac{\gamma_S}{\gamma_{THF}}$
Monomer	1	0.23	9.2±0.4	17.7±0.8
Dimer	2	0.15	30.3±0.3	58.2±0.5
Trimer	3	0.13	49±4	94±7
Pentamer	5	0.12	69±5	134±9
Heptamer	7	0.10	95±4	181±9

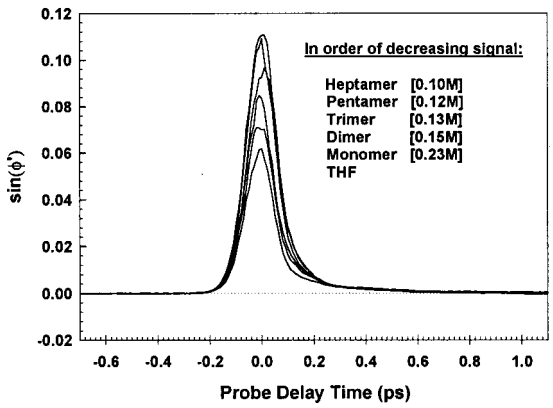

FIG. 5. Time-resolved Kerr response of THF reference/solvent and *iso*-PDA oligomer sample solutions. The molarity of each sample in THF is indicated in square brackets.

THF reference signal are presented in Fig. 5. The Kerr signal is smooth everywhere along the time-profile except at a probe delay time near 0 ps, where pump-probe coherent grating effects give rise to random on-peak noise.[26,27] This noise is significantly reduced by the averaging of several scans. Each time-resolved scan in Fig. 5 is comprised of an average of five scans. $\chi^{(3)}$ nonlinearities for samples in solution are obtained from these signals using the following equation:

$$\chi_S^{(3)} = \chi_R^{(3)} \left(\frac{\phi_S}{\phi_R} \right), \tag{7}$$

where $\chi_S^{(3)}$ and $\chi_R^{(3)}$ are, respectively, the sample and reference susceptibilities and ϕ_S and ϕ_R are, respectively, the measured rotation in polarization of the sample and reference.

A concentration test on the dimer sample was conducted to verify a linear relationship between concentration and signal, as shown in Fig. 6. Clearly, for the concentration ranges used for these *iso*-PDAs, the sample and solute may be considered noninteractive, and the samples are dilute enough to contribute additively to the $\chi^{(3)}$ signals. No evidence of aggregation was observed for any sample. The molecular sec-

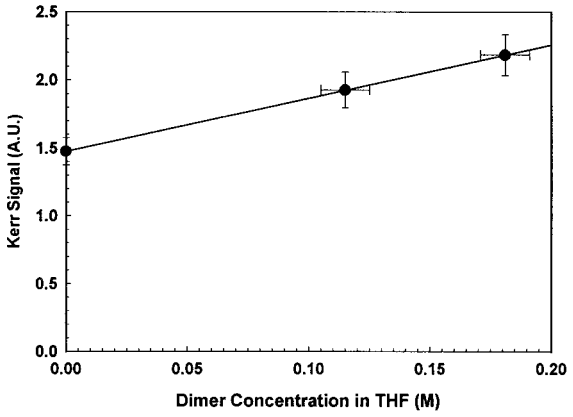

FIG. 6. Kerr response of the dimer sample as a function of concentration. The Kerr signal for the THF blank is shown at zero concentration. The other solution concentrations have uncertainties of ±0.01 M. The line is a linear fit to the data, passing through all three points.

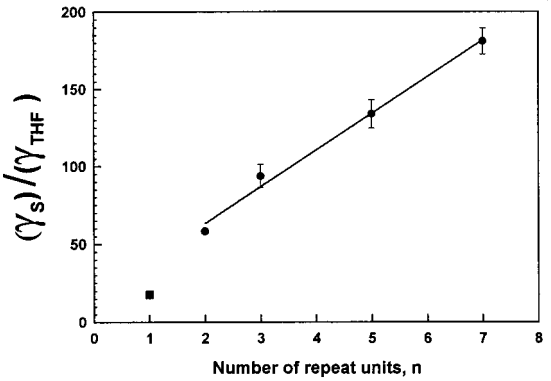

FIG. 7. Molecular second hyperpolarizability of the oligomer samples, γ_S, relative to the absolute THF hyperpolarizability, γ_{THF}, as a function of oligomer repeat length, n. The solid line is a linear fit to the data for $n=2$, 3, 5, and 7 (dimer to heptamer).

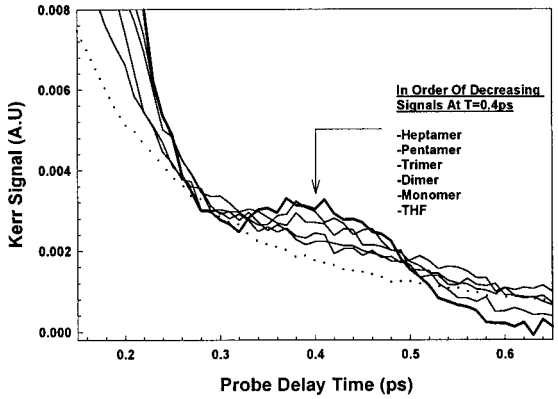

FIG. 8. Magnified view of the tail region of the Kerr response for the oligomer samples showing a noninstantaneous feature (distinct hump). The size of the hump increases with n, but remains at the same temporal position for all samples. The dotted line is a THF reference showing no deviation from smooth signal decay. To emphasize the presence of the hump, Kerr signals for each sample have been normalized to the monomer concentration. The hump does not appear at negative time delays.

ond hyperpolarizabilities for the oligomer series are obtained directly from the peak signals in Fig. 5 using

$$\gamma_S=\frac{\chi_R^{(3)}(\phi_S/\phi_R-1)}{L^4N_C}. \tag{8}$$

We use THF as a reference for all samples. Using the treatment given in Sec. II, we obtain a reference value of $\chi^{(3)}{}_R=2.1\times10^{-14}$ esu. It should be noted that $\chi^{(3)}{}_R$ is not $\chi^{(3)}{}_{\mathrm{THF}}$, as it includes contributions of the quartz cuvette.[43] Separating the effects of the sample holder yields $\chi^{(3)}{}_{\mathrm{THF}}=(1.2\pm0.3)\times10^{-14}$ esu and $\gamma_{\mathrm{THF}}=(5.2\pm1.3)\times10^{-37}$ esu,[44] which compare reasonably well with values such as $\chi^{(3)}{}_{\mathrm{THF}}=3.7\times10^{-14}$ esu ($\lambda=620$ nm)[29] and $\gamma_{\mathrm{THF}}=4.8\times10^{-37}$ esu[45] reported elsewhere. Final γ values for the samples may be found in Table I and are plotted in Fig. 7. Sample hyperpolarizabilities are calculated from the peak DOKE signals. The peak signals are at zero probe delay time, implying that the ultrafast electronic response is the most significant contributor to the oligomer nonlinearities.

In solution, unless the samples exhibit marked differences in nonlinear molecular dynamics from the solvent, the time-resolved excitation profiles will follow that of the solvent. The THF signal shows a nearly symmetric excitation attributed to the purely electronic polarizations. There is a small, noninstantaneous component to the signal. This component is due to the small asymmetry in THF and is attributed to nuclear responses. On initial inspection of the sample signals, it appears that their excitation profiles follow that of the THF reference, showing no inherit long-time dynamics. However, as seen in Fig. 8, close inspection clearly reveals a feature in the response tail that can be described as a distinct hump that arises out of the otherwise smooth signal decay tail. This feature is unique to the oligomer samples as it is clearly absent from the solvent response. Furthermore, this excitation appears to have a fairly quick rise time as is seen from the sharp ''kink'' in the heptamer signal. This feature is very small, at a little less than 1% of the peak electronic signal, and cannot at present be separated from the relaxing signal tail. In addition, the feature is seen to grow in strength from the monomer to the heptamer, yet it remains at the same delay time for all the samples.

V. DISCUSSION

In these compounds, the longest linearly conjugated path does not increase by increasing the number of repeat units. Instead, the number of fixed-length linearly conjugated paths increases as shown by the thick, solid line in Fig. 3. Thus, we no longer have a molecule that polarizes freely along its entire length. This property significantly affects the absorption energies of the oligomer. As shown in Fig. 4, *iso*-PDAs exhibit high energy edges, and are transparent at much longer chain lengths as compared to the polydiacetylenes.[46] Figure 4(a) clearly shows the samples as measured to be completely transparent at 800 nm. Furthermore, for the cross-conjugated oligomer series, $\lambda_{\max}$ values have reached saturation near the stage of the heptamer. These oligomers have the additional feature that although one dimension has lower π-delocalization along the cross-conjugated backbone, the transverse axis is hatched with linearly conjugated arms affording increases in γ (compared to the monomer) without significant reduction of the optical transparency.

As expected, the molecular hyperpolarizability increases as a function of oligomer length. As seen in Fig. 7, the *iso*-PDA series shows an order of magnitude increase in γ from the monomer to the heptamer. This is consistent with the increase in the number of fixed-length linearly conjugated paths as the number of repeat units in the oligomer is increased. The effect of adding π-delocalization paths is expected to produce a linear increase in γ as a function of n, the number of repeat units in the molecule. A linear fit for the values from dimer to heptamer was performed and is presented in Fig. 7. Clearly, the monomer sample has a much lower nonlinearity than the other samples in the series. This is due to the fact that the linear-conjugation path does not reach its maximum length until the dimer sample (see Fig. 3). For $n\geqslant2$ in the oligomer series, the longest linearly con-

jugated path length is fixed and constant, but larger than that of the monomer. Indeed, the nonlinearities of these samples seem to be governed by π-communication along the linearly conjugated paths. This is seen from the linear increase in sample hyperpolarizabilities as repeat units are added. Additional communication along the cross-conjugated backbone might be expected to give a superlinear curve in Fig. 7. Such an increase is not observed for this oligomer series. Increasing the number of repeat units to $n=9-15$ should yield more conclusive trends in sample hyperpolarizabilities, perhaps resolving any effects on the nonlinearities arising from electronic communication along the cross-conjugated backbone.

Noninstantaneous behavior is observed in the samples, as shown in Fig. 8. This behavior arises in the oligomer signals roughly 0.4 ps after maximum pump-probe overlap and is not present in the solvent signal, eliminating the possibility that this hump is an experimental artifact in the pump-probe DOKE setup. In the heptamer sample, this feature appears as a kink in the decay profile, illustrating the quick rise time of this feature. The low signal and limited resolution currently prevent further analysis, and the origin of this feature is not fully understood at this time. However, future studies, especially with *iso*-PDAs extended to longer chain length, should yield better resolution of this feature.

VI. CONCLUSIONS

We have studied the third-order nonlinearities of a novel, cross-conjugated, *iso*-polydiacetylene-based oligomer series as a function of the number of repeat units. The measurements were performed using a unique optical Kerr-gate detection technique called differential optical Kerr effect, or DOKE, which represents a modification of the OHD-OKE scheme. Values of $\gamma_{\text{monomer}}=(9.2\pm0.4)\times10^{-36}$ esu, $\gamma_{\text{dimer}}=(30.3\pm0.3)\times10^{-36}$ esu, $\gamma_{\text{trimer}}=(49\pm4)\times10^{-36}$ esu, $\gamma_{\text{pentamer}}=(69\pm5)\times10^{-36}$ esu, and $\gamma_{\text{heptamer}}=(95\pm4)\times10^{-36}$ esu were obtained, relative to a THF reference of $\gamma_{\text{THF}}=(0.52\pm0.12)\times10^{-36}$ esu. These compounds show a rise in the molecular second hyperpolarizability, γ, as the chain length is increased from the monomer to the heptamer. This increase in γ can be attributed to an increase in the number of fixed-length linearly conjugated paths. No added contribution to the nonlinear response attributable to the cross-conjugated backbone has been observed. In addition, an interesting feature in the sample signals was observed about 0.4 ps after the instantaneous electronic Kerr response. This feature suggests molecular dynamics effects, but at present the source of the response in unaccounted for. Extension of the oligomer series to $n=15$, for example, should provide more concrete trends in sample nonlinearities. The study of longer oligomer lengths is in progress.

ACKNOWLEDGMENTS

This research was supported by NSERC, CFI, IIPP, ASRA, and CIPI.

[1] G. I. Stegeman and A. Miller, in *Photonics in Switching (Vol. I), Background and Components*, edited by J. E. Midwinter (Academic, Boston, 1993).
[2] J. L. Bredas, C. Adant, P. Tackx, and A. Persoons, Chem. Rev. **94**, 243 (1994).
[3] P. N. Prasad and D. J. Williams, *Introduction to Nonlinear Optical Effects in Molecules and Polymers* (Wiley Interscience, New York, 1991), pp. 300–302.
[4] D. Neher, A. Kaltbeitzel, A. Wolf, C. Bubeck, and G. Wegner, J. Phys. D **24**, 1193 (1991).
[5] G. P. Agrawal, C. Cojan, and C. Flytzanis, Phys. Rev. B **17**, 776 (1978).
[6] C. Bubeck, in *Electronic Materials: The Oligomer Approach*, edited by K. Mullen and G. Wegner (Wiley-VCH, Chichester, 1998).
[7] L.-T. Cheng, W. Tam, S. R. Marder, A. E. Stiegman, G. Rikken, and C. W. Spangler, J. Phys. Chem. **95**, 10643 (1991).
[8] C. Bosshard, Habilitation Thesis, Institute of Quantum Electronics, Zürich, Switzerland, 1998.
[9] C. Bosshard, R. Preiter, P. Gunter, R. R. Tykwinski, M. Schreiber, and F. Diederich, Adv. Mater. **3**, 231 (1996).
[10] R. R. Tykwinski, U. Gubler, R. E. Martin, F. Diederich, C. Bosshard, and P. Gunter, J. Phys. Chem. B **102**, 4451 (1998).
[11] H. S. Nalwa, in *Nonlinear Optics of Organic Molecules and Polymers*, edited by H. S. Nalwa and S. Miyata (CRC, New York, 1997), pp. 571–797.
[12] *Characterization Techniques and Tabulations for Organic Nonlinear Optical Materials*, edited by M. G. Kuzyk and C. W. Dirk (Dekker, New York, 1998).
[13] S. Y. Kim, M. Lee, and B. H. Boo, J. Chem. Phys. **109**, 2593 (1998).
[14] P. Maslak, Adv. Mater. **6**, 405 (1994).
[15] S. C. Ciulei and R. R. Tykwinski, Org. Lett. **2**, 3607 (2000).
[16] P. P. Ho and R. R. Alfano, Phys. Rev. A **20**, 2170 (1979).
[17] A. A. Ho, in *Semiconductors Probed by Ultrafast Laser Spectroscopy*, edited by R. R. Alfano (Academic, New York, 1984), Vol. II, pp. 409–439.
[18] S. Guha, C. C. Frazier, P. L. Porter, K. Kang, and S. E. Finberg, Opt. Lett. **14**, 952 (1989).
[19] M. G. Kuzyk, R. A. Norwood, J. W. Wu, and A. F. Garito, J. Opt. Soc. Am. B **6**, 154 (1989).
[20] Y. Pang, M. Samoc, and P. N. Prasad, J. Chem. Phys. **94**, 5282 (1991).
[21] V. Philippart, M. Dumont, J. M. Nunzi, and F. Charra, Appl. Phys. A: Solids Surf. **56**, 29 (1993).
[22] S. R. Vigil and M. G. Kuzyk, J. Opt. Soc. Am. B **18**, 679 (2001).
[23] P. N. Butcher and D. Cotter, *The Elements of Nonlinear Optics* (Cambridge University Press, Cambridge, 1990), pp. 306–308.
[24] See Ref. 23, pp. 79–85.
[25] M. D. Levenson and G. L. Easley, Appl. Phys. **19**, 1 (1979).
[26] D. McMorrow, W. T. Lotshaw, and G. A. Kenney-Wallace, IEEE J. Quantum Electron. **24**, 443 (1988).
[27] C. Kalpouzos, W. T. Lotshaw, D. McMorrow, and G. A. Kenney-Wallace, J. Phys. Chem. **91**, 2028 (1987).
[28] M. E. Orczyk, M. Samoc, J. Swiatkiewicz, N. Manickam, M. Tomoaia-Cotisel, and P. N. Prasad, Appl. Phys. Lett. **60**, 2837 (1992).
[29] M. E. Orczyk, M. Samoc, J. Swiatkiewicz, and P. N. Prasad, J. Chem. Phys. **98**, 2524 (1993).
[30] K. Kamada, M. Ueda, T. Sakaguchi, K. Ohta, and T. Fukumi, Chem. Phys. Lett. **263**, 215 (1996).
[31] K. Kamada, M. Ueda, T. Sakaguchi, K. Ohta, and T. Fukumi, J. Opt. Soc. Am. B **15**, 838 (1998).
[32] K. Kamada, M. Ueda, K. Ohta, Y. Wang, K. Ushida, and Y. Tominaga, J. Chem. Phys. **109**, 10948 (1998).
[33] T. Hattori, A. Terasaki, T. Kobayashi, T. Wada, A. Yamada, and H. Sasabe, J. Chem. Phys. **95**, 937 (1991).
[34] B. J. Loughnane and J. T. Fourkas, J. Phys. Chem. B **102**, 10288 (1998).
[35] B. J. Loughnane, A. Scodinu, R. A. Farrer, J. T. Fourkas, and U. Mohanty, J. Chem. Phys. **111**, 2686 (1999).
[36] S. Kinoshita, Y. Kai, and Y. Watanabe, Chem. Phys. Lett. **301**, 183 (1999).
[37] A. Idrissi, M. Ricci, P. Bartolini, and R. Rhigini, J. Chem. Phys. **111**, 4148 (1999).
[38] Q. Wu, M. Litz, and X.-C. Zhang, Appl. Phys. Lett. **68**, 2924 (1996).
[39] K. P. H. Lui and F. A. Hegmann, Appl. Phys. Lett. **78**, 3478 (2001).
[40] A. Willetts, J. E. Rice, and D. M. Burland, J. Chem. Phys. **97**, 7590 (1992).
[41] T. Hattori and T. Kobayashi, J. Chem. Phys. **94**, 3332 (1991).
[42] Y. Zhao and R. R. Tykwinski, J. Am. Chem. Soc. **121**, 458 (1999).

[43] Note: A full discussion of signal analysis and blank separation is beyond the scope of this article. Suffice it to say that in any equation provided in this work, $\chi^{(3)}{}_R$ and ϕ_R refer to signals that include the sample holders, whereas $\chi^{(3)}{}_{\mathrm{THF}}$ and ϕ_{THF} refer to pure THF values.

[44] Note: The uncertainty in these values comes from uncertainties in many pulse-shape/power diagnostics, as well as signal analysis. The error in γ reported for the samples is due to uncertainties in signal analysis alone since a precise $\chi^{(3)}$ is assumed.

[45] P. L. Porter, S. Guha, K. Kang, and C. C. Frazier, Polymer **32**, 1756 (1991).

[46] H. J. Byrne, W. Blau, R. Giesa, and R.C. Schulz, Chem. Phys. Lett. **167**, 484 (1990); R. Giesa, M. Klapper, and R. C. Schultz, Makromol. Chem., Macromol. Symp. **44**, 1 (1991).